Comparison of the FLUKA calculations with CAPRICE94 data on muons in atmosphere

G. Battistoni[a], A. Ferrari[a,b], T. Montaruli[c]
P. R. Sala[a,b]

a) INFN and Dipartimento di Fisica dell' Universitá, 20133 Milano, Italy
b) now at CERN, Geneva, Switzerland
c) INFN and Dipartimento di Fisica dell' Universitá, 70126 Bari, Italy
and INFN Laboratori Nazionali di Frascati, 00044 Frascati, Italy

Abstract

In order to benchmark the 3-dimensional calculation of the atmospheric neutrino flux based on the FLUKA Monte Carlo code, muon fluxes in the atmosphere have been computed and compared with data taken by the CAPRICE94 experiment at ground level and at different altitudes in the atmosphere. For this purpose only two additions have been introduced with respect to the neutrino flux calculation: the specific solar modulation corresponding to the period of data taking and the bending of charged particles in the atmosphere. Results are in good agreement with experimental data, although improvements in the model are possible. At this level, however, it is not possible to disentangle the interplay between the primary flux and the interaction model.

1 Introduction

Recently, a new atmospheric neutrino flux calculation, based on the FLUKA Monte Carlo model[1], has been proposed[2]. This new calculation has been produced with the aim to introduce a high level of refinement in the modeling of all aspects of shower calculations in atmosphere, from particle production to particle transport. The need for a 3-Dimensional approach has also been demonstrated. For example, considering as reference the Bartol flux calculation[3], and accounting for the differences in the 1-D and 3-D approaches, the FLUKA results are, for $E_\nu > 1$ GeV, $\sim$15% lower. This has been obtained for the same input primary spectrum and the reduction is present also at energies far from effects due to geomagnetic field. This was attributed to the differences between particle production models[4]. An almost identical difference is present with respect to the Honda et al. simulation[5] (HKKM in the following), but in this case the input primary spectrum is not the same and is believed to be the main source of the discrepancy.

Since at present there is not yet a firm experimental determination of the absolute neutrino flux, one of the possible ways to check the validity of shower calculations, and of the corresponding interaction models, is to compare the results for other detectable particles, like for instance muons. Muons have a direct link with neutrinos through the decay mechanisms, which are rather well known. Unlike neutrinos, not all muons produced in atmospheric showers are available at ground level, due to energy loss and decay along their path. Therefore, the data taken at different altitudes by means of balloon–born detectors are of particular interest. In this respect, the data obtained by the CAPRICE experiment are of particular interest and considered among the most reliable by the scientific community. We are interested in particular to the data taken at Lynn Lake in 1994 and published in [6]. In this paper we describe the results of the comparison of our FLUKA calculations with this data set, showing that, under the assumption concerning the validity of the input primary spectrum adopted so far, a good agreement with these muon data is achieved.

Another neutrino flux calculation has been recently proposed[7], with a model capable of obtaining a successful comparison with the CAPRICE data. In this case the normalization of the resulting neutrino flux is different from the FLUKA one, depending on neutrino flavor and energy, but with the general trend of producing a 20 – 25% lower normalization in the sub–GeV region. According to the authors, when switching from their particle production model to the Bartol one the resulting neutrino fluxes obtained with their code (CORT) increase by a factor exceeding 50% in the Sub–GeV range. They conclude that their model, which is able to reproduce the muon fluxes in the atmosphere, predicts significantly lower neutrino fluxes than those currently used in the experimental analyses (mostly the Bartol[3] and HKKM[5] computations).

2 Monte Carlo setup

The FLUKA code [1] is a general purpose Monte Carlo code for the interaction and transport of particles. It is built and maintained with the aim of including the best possible physical models in terms of completeness and precision. It contains detailed models of electromagnetic, hadron–hadron and hadron–nucleus interactions, covering the range from the MeV scale to the many–TeV one. Extensive benchmarking against experimental data has been produced (see the references in [1]). In view of applications for cosmic ray physics, we have implemented in the FLUKA environment a 3–Dimensional spherical representation of the whole Earth and of the surrounding atmosphere. The latter is described by a by a proper mixture of N, O and Ar, arranged in 100 concentric spherical shells, whose densities follow the known profile of the USA "standard atmosphere". This is the standard choice in neutrino flux calculations, although we are aware that important differences exist as a function of latitude and season. For a muon flux calculation the specific features of the local geographical site and the actual situation on the days of measurement could be relevant for a fully significant comparison with data. We have also tried to set the boundaries between the atmospheric shells in such a way to reproduce as

much as possible the different "flux weighted average depths" at which the CAPRICE94 measurements were reported. Considering our discrete structure and the adopted atmosphere profile, we evaluated a systematic error on the atmospheric depth of less than few percent.

The starting point of any calculation of particle fluxes in the atmosphere is the primary flux. In order to allow a direct comparison with previously published computations, we used the fit of all–nucleon flux proposed by the Bartol group[3]. This flux has also the merit that, at least up to about hundred GeV it is quite close to the recent measurements of proton primaries performed by BESS[8] and AMS[9]. A comparison with these data sets is shown in Fig. 1, where the all–nucleon spectrum has been divided in the free–proton and bounded–nucleon components. To the bounded–nucleon component, mass groups heavier than helium contribute. The sum of such contributions, taken from ref. [10], are represented by a continuous line. Nuclei are treated in the framework of the superposition model, namely a nucleus of mass number A, and total energy E_0 is considered to be equivalent to A nucleons each having energy E_0/A. At present, this is the approach followed in all other neutrino calculations, except the case of ref.[7], where a Glauber-like model is used for the primary nuclear component.

For the purpose of the present calculation, we have modified the spectrum in order to take into account the solar modulation at the time of the experimental measurement (August 8th 1994). In order to do that, we have followed the modeling of ref. [11]. First, a Local Interstellar Spectrum has been derived from the Bartol spectrum at solar minimum, and than it has been modulated back to the desired level according to the counting rate of the Climax neutron monitor. The effect of solar modulation on all–nucleon spectrum is shown in Fig. 2. Primary particles, sampled from the continuous energy spectrum, are injected at the top of the atmosphere, at about 100 km of altitude.

The primary flux is assumed to be uniform and isotropic far from the Earth, and it is locally modified by the effects of the geomagnetic field[12] and solar modulation. Contrary to our previous neutrino flux calculation we have switched on the local magnetic field also during shower development, in order to allow the bending of charged particle trajectories.

In the simulation we score the muon flux separately for each muon charge, at each boundary crossing between the different atmospheric shells, and at the Earth boundary as well. We have tested different acceptance cones to define the fluxes, using half-cone angles of 8, 12 and 20 degrees. At a few altitudes we have also added a cone of 50 degrees of half-aperture. The muon flux is recorded as function of laboratory momentum, in 30 logarithmic bins between 0.2 and 200 GeV/c. In order to compare our results to the experimental data, a binning of calculated fluxes has been performed to reproduce the momentum ranges considered in [6]

We have also performed simulation runs in the 1–Dimensional approximation, that is aligning all secondary particles to the primary at each interaction.

3 Results

As a first step, we have studied the dependence of simulated fluxes, at different heights, as a function of the different aperture cones. As a result we may conclude that up to 20 degrees, the simulation does not show a significant dependence on the aperture cone at all heights. In the 50 degrees cone, instead, a loss of muon flux at low muon momentum can be observed with respect to the lower apertures. As an example, in Fig. 3 the negative muon flux as a function of momentum for different aperture cones is shown at the nominal atmospheric depth of 50.7 g/cm^2 (a), corresponding to about 20.6 km of altitude (a) and at the nominal depth of 308.9 g/cm^2 (b), that is at about 9.08 km of altitude. The loss at low muon momentum at large angle is explained by muon energy loss and decay.

The comparison with the experimental data from CAPRICE is performed using the muon flux recorded in the 12 degrees half-aperture cone, the one closer to the apparatus acceptance. The results, relative to the full 3–Dimensional simulation runs, are summarized in Fig. 4 for the negative muon measurements at different depths in atmosphere and in Fig. 5 for the positive muons. The numeric values of the simulated fluxes reported in these figures are reported in Tables 3 and 4 in the Appendix, for the different detector depths. The same data are reported as a function of depth, in different momentum intervals, in Fig. 6 and 7, for negative and positive muons respectively. In order to express numerically the level of agreement between data and simulation, we report in table 1 the weighted average of ratios of Monte Carlo to experimental data at each atmospheric depth. as from Fig. 4 and 5, (thus integrating on all momentum bins). In a similar way, table 2 shows the average ratios at each momentum bin (integrating on all atmospheric depths). Statistical errors have been used to calculate the weights.

We consider satisfactory the general level of agreement, also taking into account that here we are assuming that no systematic error exist for this set of experimental data. Instead, as stated before, a few percent systematics in the calculation should come from the atmospheric description. We notice a deficit in the simulation with respect to the data at very low momenta at the topmost altitude. In the case of negative muons there could be at most a 10% deficit in simulation. in the range 1.23$\div$2.0 GeV/c. Here the deficit is dominated by low values obtained at the shower depths between 100 and 170 g/cm^2, although both at 77 and 218 g/cm^2 (still close to the shower maximum) a ratio close to 1.0 is again achieved. For positive muons the maximum deficit is limited to 0.75$\div$0.97 momentum bin, again dominated by the results in the range between 100 and 170 g/cm^2. However, we want to stress that, for a given interaction model and calculation scheme, these values depend also on the choice of primary all nucleon spectrum. Furthermore we also expect that our assumption on the total absence of systematics in the experimental data is probably too optimistic. With the present level of statistical error we cannot identify systematic problems in the μ^+/μ^- ratio at these altitudes.

Fig. 8 shows the comparison with the measurement at ground level. Numerical values are given in table 5. In this case the flux have been calculated in momentum bins which are slightly different with respect to those of experimental data. Therefore, in order to evaluate the level of agreement, we calculated the ratios of simulated fluxes to the

Atmospheric Depth (g/cm^2)	MC/Exp. Data (μ^-)	MC/Exp. Data (μ^+)
3.99	0.84 ± 0.06	0.78 ± 0.07
25.7	0.97 ± 0.07	1.00 ± 0.08
50.7	1.00 ± 0.05	1.06 ± 0.07
77.3	1.04 ± 0.06	0.96 ± 0.07
104.1	0.94 ± 0.05	0.91 ± 0.04
135.3	0.94 ± 0.05	0.92 ± 0.06
173.8	0.98 ± 0.05	0.92 ± 0.06
218.8	1.03 ± 0.04	1.11 ± 0.07
308.9	0.97 ± 0.06	0.83 ± 0.07
463.7	0.96 ± 0.05	0.97 ± 0.08
709	1.04 ± 0.06	1.27 ± 0.19
1000	0.99 ± 0.03	0.79 ± 0.04

Table 1: Weighted average ratios of simulated to experimental data for different atmospheric depths and integrating on the different momentum ranges.

Muon momentum (GeV/c)	MC/Exp. Data (μ^-)	MC/Exp. Data (μ^+)
0.3–0.53	1.02 ± 0.05	0.92 ± 0.04
0.53–0.75	0.97 ± 0.03	0.94 ± 0.04
0.75–0.97	1.04 ± 0.05	0.83 ± 0.03
0.97–1.23	1.00 ± 0.05	0.94 ± 0.05
1.23–1.55	0.88 ± 0.04	1.00 ± 0.06
1.55–2.0	0.91 ± 0.04	0.98 ± 0.06
2.0–3.2	0.97 ± 0.04	—-
3.2–8.0	1.02 ± 0.03	—-
8.0–40.0	0.96 ± 0.05	—-

Table 2: Weighted average ratios of simulated to experimental data in different momentum bins and integrated on the different atmospheric depths.

values at the same momentum (above 0.3 GeV/c) taken from the phenomenological fits to experimental data shown as continuous lines in Fig. 8. The distribution of these ratios are shown in Fig. 9. Here, the present results could point out a possible deficit in the calculated μ^+'s with respect to the μ^-. However, it is again important to remember that also the modeling of primary spectrum does affect this result, through the neutron to proton ratio which in turn is determined by the relative abundances of nuclei and free nucleons.

In order to understand the possible relevance of the 3–dimensional simulation setup we have also analyzed data obtained with the 1–dimensional runs. From this comparison we can conclude that differences exist at low muon momenta, where a noticeable excess of muons is produced in the 1–Dimensional simulations. As an example, we show in Fig. 10 the calculated negative muon flux as a function of atmospheric depth in 4 different momentum intervals for the 1–Dimensional and 3–Dimensional simulations. Fig. 11 shows similar results for positive muons. In the lowest momentum bins, the 1–D simulation yields a larger muon flux. We attribute the difference between the 1–D and 3–D cases to a different path length distribution of muons: the inclusion of kinematic production angle, together with particle bending in the geomagnetic field, brings to an increase of path length and, as a consequence, to a larger decay probability. This argument has been discussed by the Bartol group and other authors in ref. [14], after that preliminary comparisons of the Bartol 1–D results with CAPRICE data were showing a significant excess in the calculated flux in the low momentum region, as also reported in [15]. However, in our opinion it is more probable that the main reason for the excess in that calculation was an excess of pion multiplicity. In fact the Bartol group is preparing an improved version of their interaction model which seems to yield charged pion multiplicities closer to those from the FLUKA model[16]. Other differences in Monte Carlo calculations of muons in the atmosphere between the 1–D and 3–D case have been already reported in ref.[17], where the original interaction model from Bartol was used: however, in this case, significant excess of calculated muons as compared to HEAT data was observed at high altitude for a wide range of momentum. This reinforces our interpretation on the excess of multiplicity in the first Bartol model.

4 Conclusions

The results presented here demonstrate that the FLUKA model can reasonably reproduce the muon fluxes in the atmosphere as measured by the CAPRICE experiment. Of course, the accuracy and reliability of such a comparison depends also on the choice of the atmospheric model and, mostly, on the assumptions concerning the primary spectrum and the geomagnetic cutoff. In particular we are aware that the Bartol all nucleon flux should be slightly modified in order to be compatible with the latest data on primaries[19]. Furthermore, one should also consider that also the present data from balloon experiments might be affected by systematic errors which could be $\lesssim 10\%$[18]. In this work we are are relying on the choices adopted for our calculation of neutrino fluxes in atmosphere, and therefore

we can use the results of the present study to at least partially validate the neutrino results, due to the strong link between muon and neutrino production. As a result we can conclude that, having used the same primary spectrum, the normalization difference in neutrino flux with respect to the Bartol results cannot be attributed to an insufficient particle production yield in the shower development in the FLUKA model. As far as absolute normalization is concerned, the muon data considered here allow to conclude that the FLUKA calculation should have at maximum a 10% error in the neutrino energy range up to few GeVs. Of course this last statement is strongly related to the choice of the primary spectrum, and it is not possible at this stage to disentangle this factor from the feature of the FLUKA interaction model, which is otherwise independently benchmarked against particle production data. We wish to stress that data taken in controlled conditions at accelerators should remain the main constraint for any interaction model to be used for particle production in atmosphere. In particular we remind that hadron–Nucleus and Nucleus–Nucleus interactions in the energy range $1 \div 30$ GeV are still insufficiently known to allow the construction of a fully reliable model. The check with measured fluxes of different particles in atmosphere remains however relevant in order to verify that all other ingredients of the simulation setup are taken into account correctly.

Another conclusion of this work is that 3–Dimensional effects are of some important also for low energy muons. If we assume that our 3–D vs. 1–D effect is correct, there could be implications for the results recently presented by Fiorentini et al., in [7]. However, the significant differences in SubGev neutrino fluxes between the results of [7] and those from the FLUKA calculation[2] seem hard to explain on the basis of a geometrical effect or of differences in the primary spectrum. The main difference should be the interaction model, but then it is still difficult to explain why different neutrino fluxes arise from calculations yielding reasonable reproduction of the same data on muon fluxes, a part from technical errors or, maybe, from important differences in muon energy loss and decay, but at this stage this is just a guess. As far as FLUKA is concerned the energy loss models have been obviously widely cross–checked and verified after many years of practice in precision problems like radiation shielding, dosimetry and other radio–biological applications. Muon decay with correct polarization effects has been checked together with the Bartol group.

Acknowledgments

We wish to thank M. Boezio and M. Circella for the help received in understanding the muon experiments and their data.

References

[1] A. Ferrari and P.R. Sala, ATLAS internal note ATL-PHYS-97-113 (1997) accessible through the CERN preprint server; Proc. of the *Workshop on Nuclear Reaction Data and Nuclear Reactors Physics, Design and Safety*, ICTP, Miramare-Trieste, Italy,

15 April–17 May 1996, Proceedings published by World Scientific, A. Gandini, G. Reffo eds, Vol. 2, p. 424, (1998).

[2] G. Battistoni et al., Nuclear Phys. B (Proc. Suppl.) **70** (1998) 358; G. Battistoni et al., Astrop. Phys. **12** (2000) 315. FLUKA flux tables are available in http://www.mi.infn.it/~battist/neutrino.html.

[3] V. Agrawal et al., Phys. Rev. **D53** (1996) 1314; G. Barr et al., Phys. Rev. **D39** (1989) 3532; T. K. Gaisser and T. Stanev, Proc. of the 24th ICRC (Rome, 1995), vol.**1**, 694.

[4] G. Battistoni, hep-ph/0012268, and Nucl. Phys. Proc. Suppl. **100** (2001) 101 *(Proc of the Neutrino Oscillation Workshop 2000, Otranto, Sep. 2000).*

[5] M. Honda et al., Phys. Rev. **D52** (1995) 4985.

[6] M. Boezio et al., Phys. Rev. **D62** (2000) 032007.; J. Kremer et al., Phys. Rev. Lett. **83** (1999) 4241.

[7] G. Fiorentini, V.A. Naumov, F.L. Villante, hep-ph/0103322.

[8] T. Sanuki et al., Astrophys. J. **545** (2000) 1135.

[9] J. Alcaraz et al., Phys. Lett. **B472** (2000) 215.

[10] B. Wiebel-Sooth, P. Biermann and H. Meyer, astro-ph/9709253

[11] G.D. Badhwar and P.M. O'Neill, Adv. Space Res. Vol. **17**, No. 2 (1996) 7.

[12] In the FLUKA calculations of particle fluxes in atmosphere we have used the IGRF (International Geomagnetic Reference Field) available from NASA/NSSDC.

[13] The fit to atmospheric profile has been taken from T. K. Gaisser, "Cosmic Rays and Particle Physics", Cambridge University Press, Cambridge, England.

[14] T. Stanev, S. Coutu, T.K. Gaisser and G. Barr, Proc. of the 26th ICRC, Utah 1999, **Vol. 2**, 96.

[15] M. Circella, talk at the VIII Workshop on Neutrino Telescope, Venezia, Feb. 1999.

[16] R. Engel, T.K. Gaisser, P. Lipari and T. Stanev, Proc. of the 27th ICRC (Hamburg, 2001), Session HE2.02.

[17] S. Coutu et al., Phys. Rev. **D62** (2000) 032001.

[18] M. Circella, private communication.

[19] T.K. Gaisser, M. Honda, P. Lipari and T. Stanev, Proc. of the 27th ICRC (Hamburg, 2001), Session OG1.01

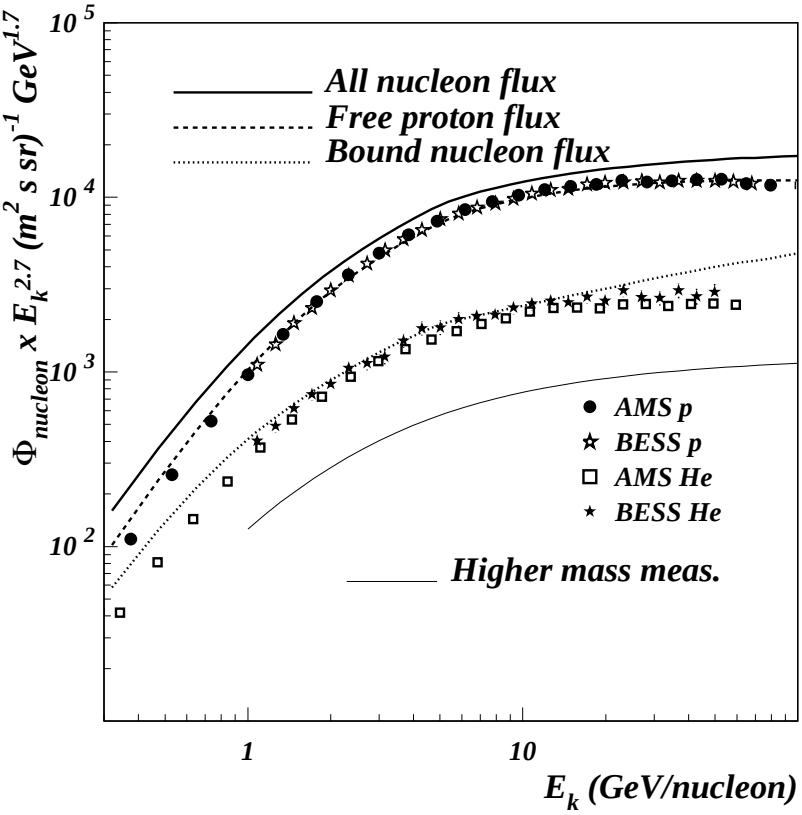

Figure 1: All-nucleon primary spectrum (from Bartol group) used for the FLUKA calculations in the atmosphere as compared to recent AMS and BESS data sets. The continuous line representing higher mass components has been derived from ref. [10].

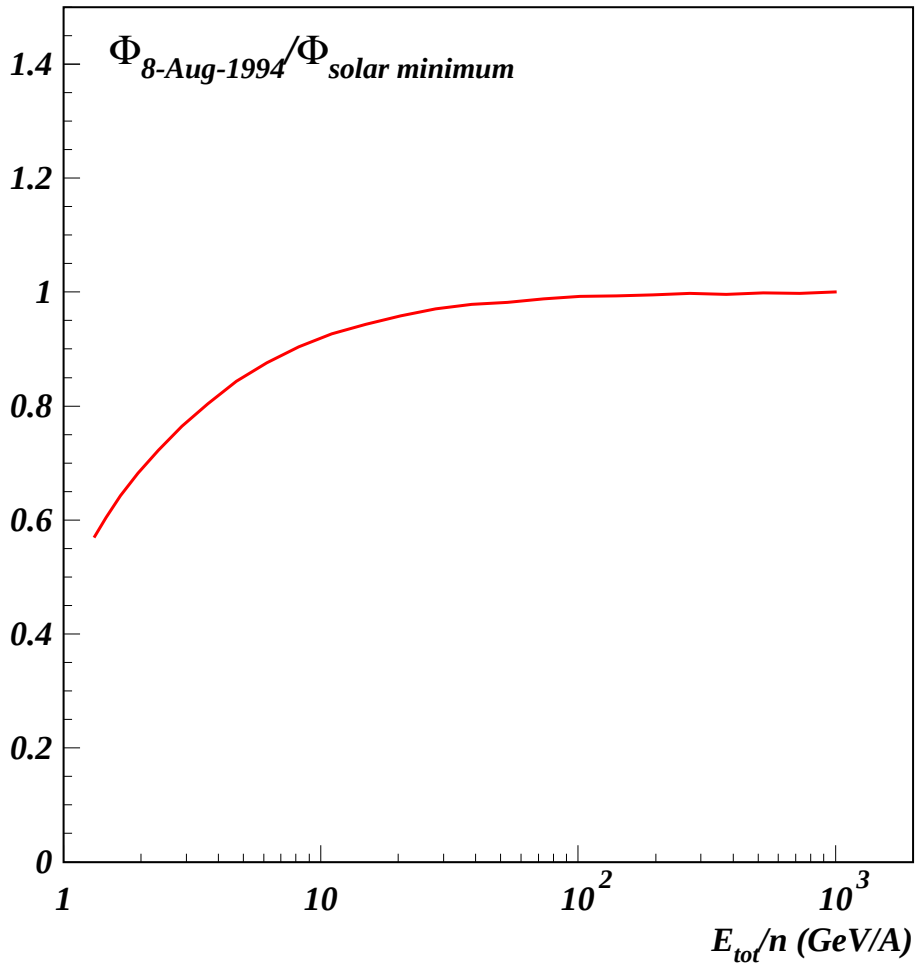

Figure 2: Ratio of all-nucleon primary spectrum modulated for the date of August 8^{th} 1994 to that at solar minimum value, as obtained using the algorithm of ref. [11].

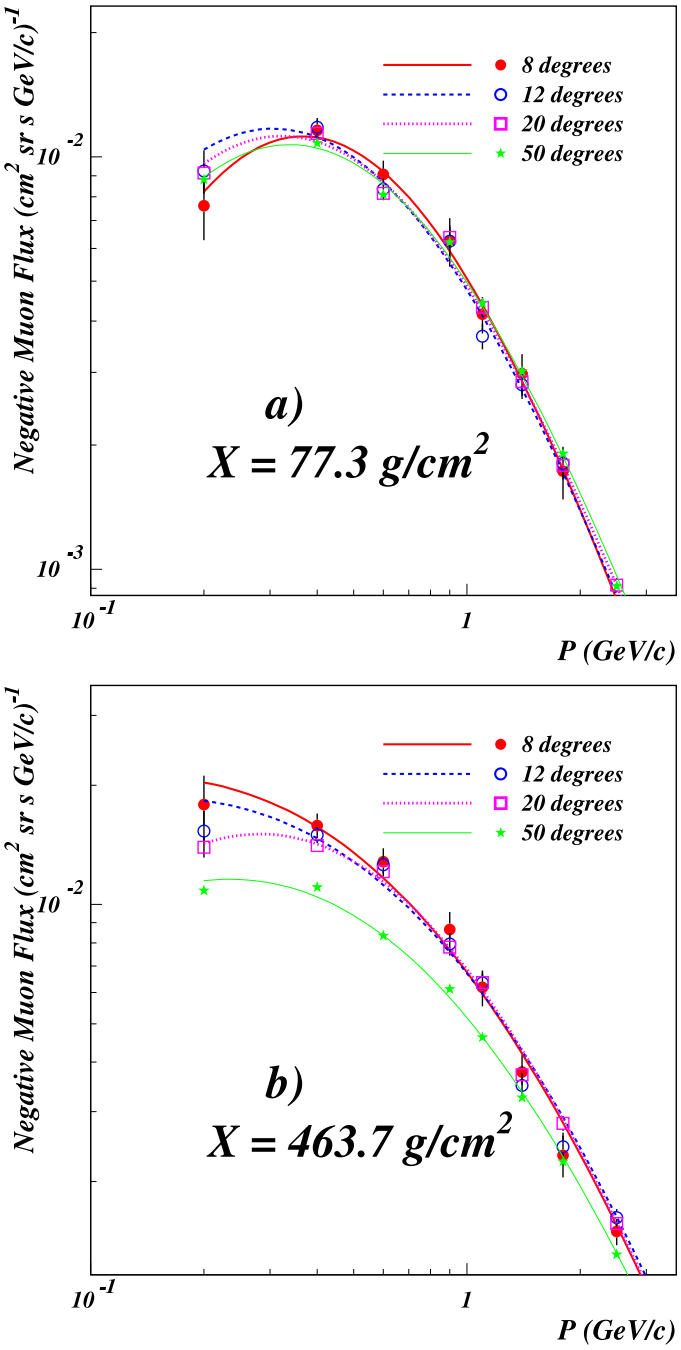

Figure 3: Calculated Negative muon flux as a function of momentum for different aperture cones is shown at the atmospheric depth of 50.7 g/cm^2 (a), corresponding to about 20.6 km of altitude (a) and at the depth of 308.9 g/cm^2 (b), that is at about 9.08 km of altitude). The lines are phenomenological fits meant to guide the eye.

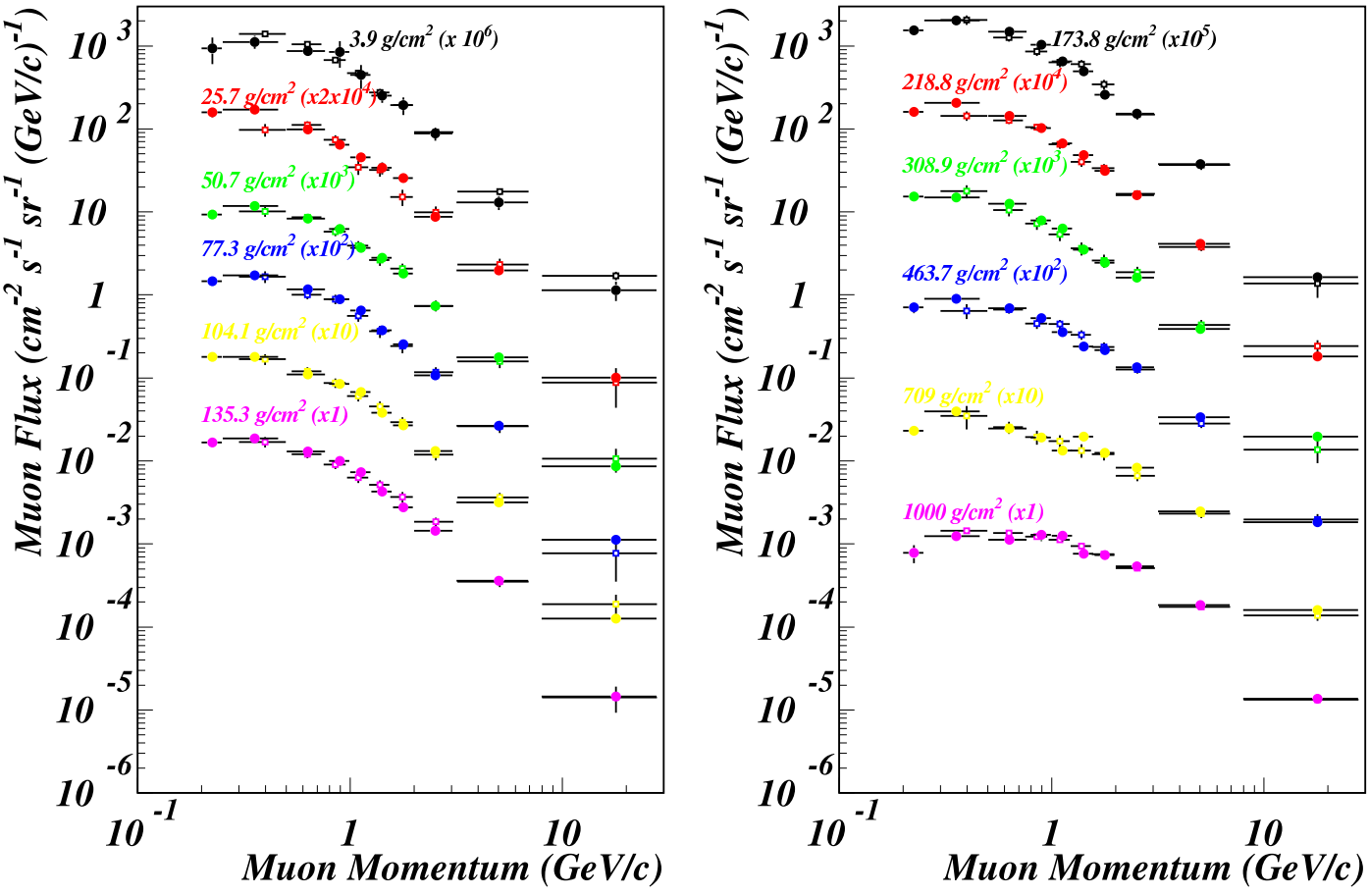

Figure 4: Comparison between simulated and detected negative muon flux as a function of momentum for different atmospheric depths.

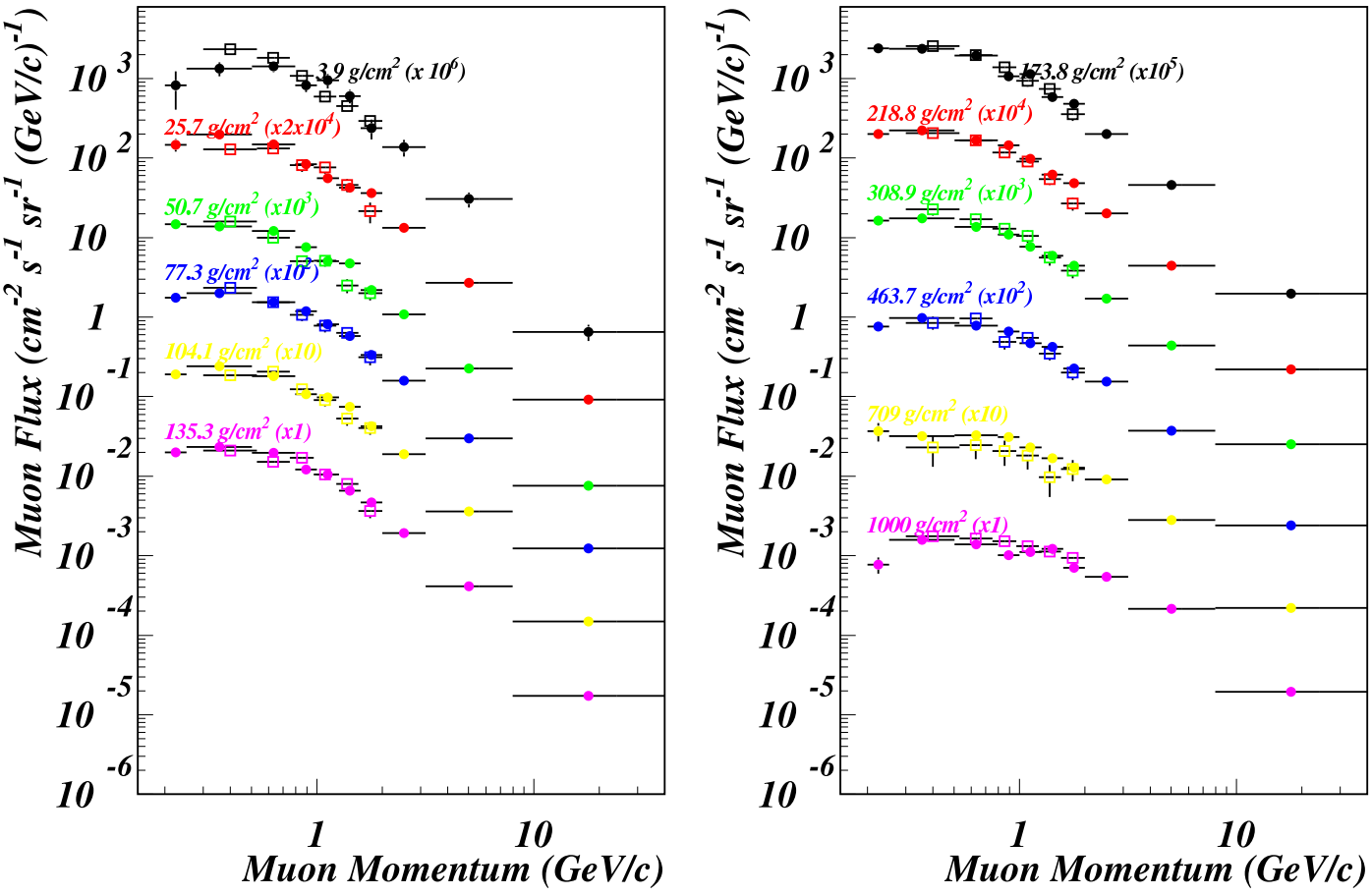

Figure 5: Comparison between simulated (small full symbols) and detected positive muon flux (open symbols) as a function of momentum for different atmospheric depths.

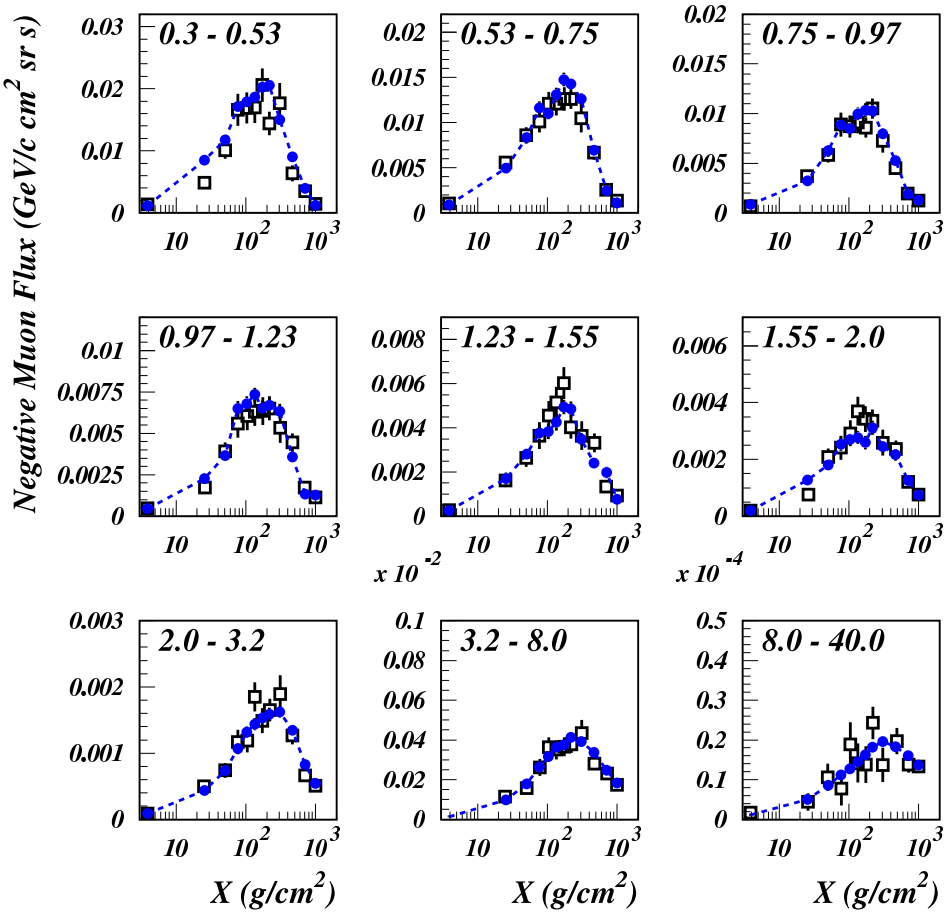

Figure 6: Comparison between simulated (full symbols) and detected negative muon flux (open symbols) as a function of atmospheric depth, for different momentum bins. The dotted line is draw to guide the eye.

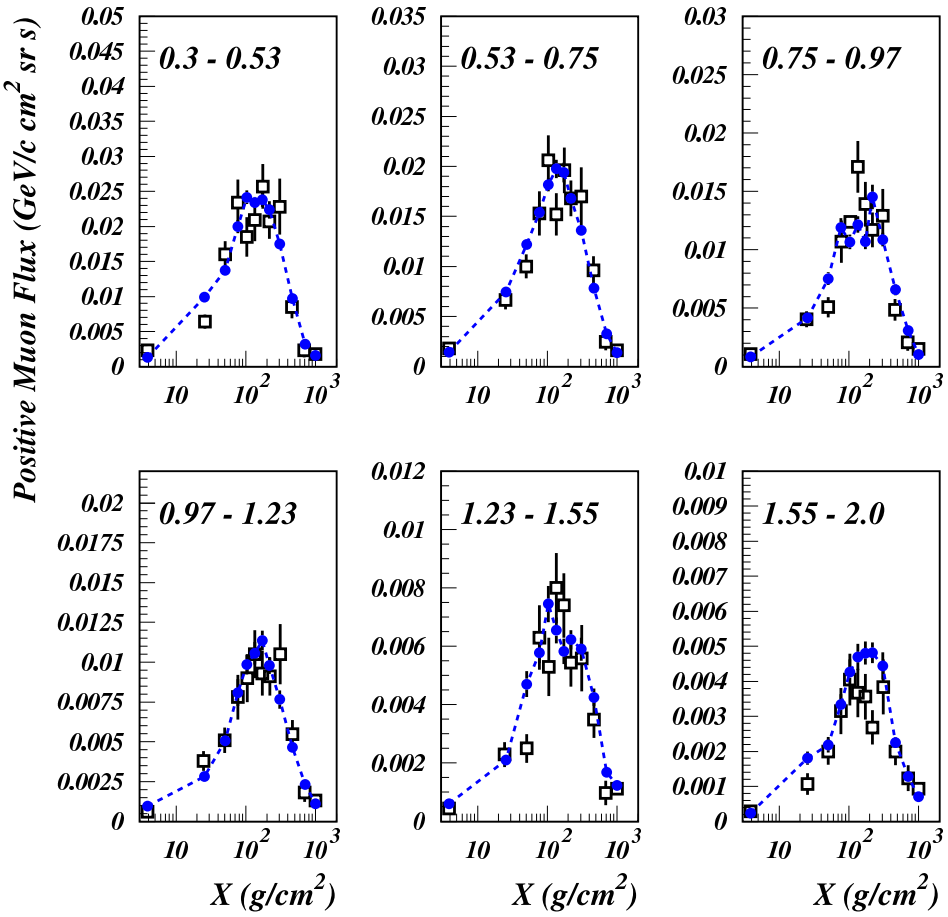

Figure 7: Comparison between simulated (full symbols) and detected positive muon flux (open symbols) as a function of atmospheric depth, for different momentum bins. The dotted line is drawn to guide the eye.

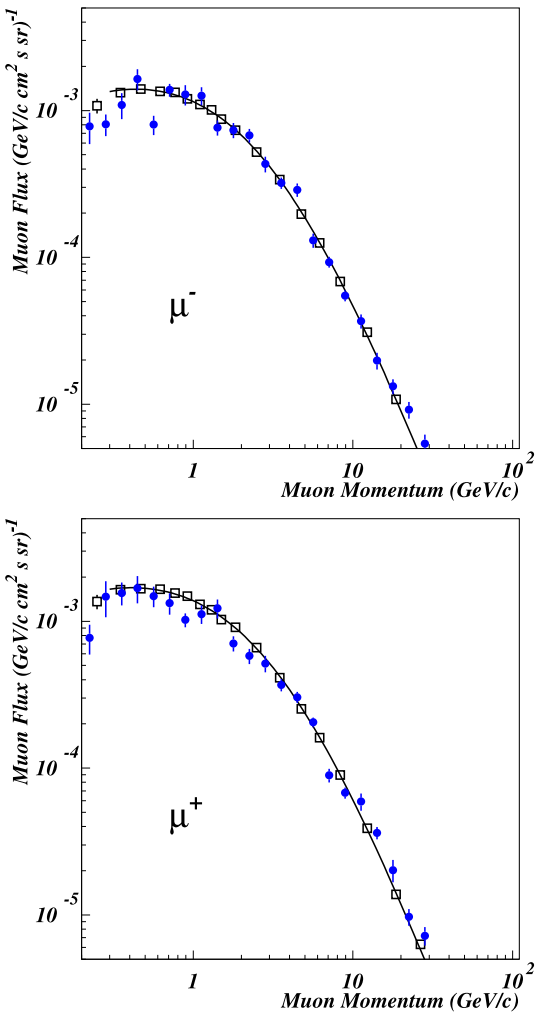

Figure 8: Comparison between simulated (full symbols) and detected (open symbols) negative and positive muon fluxes as a function of momentum at ground level. The continuous lines are phenomenological fits to the experimental data (above 0.3 GeV/c).

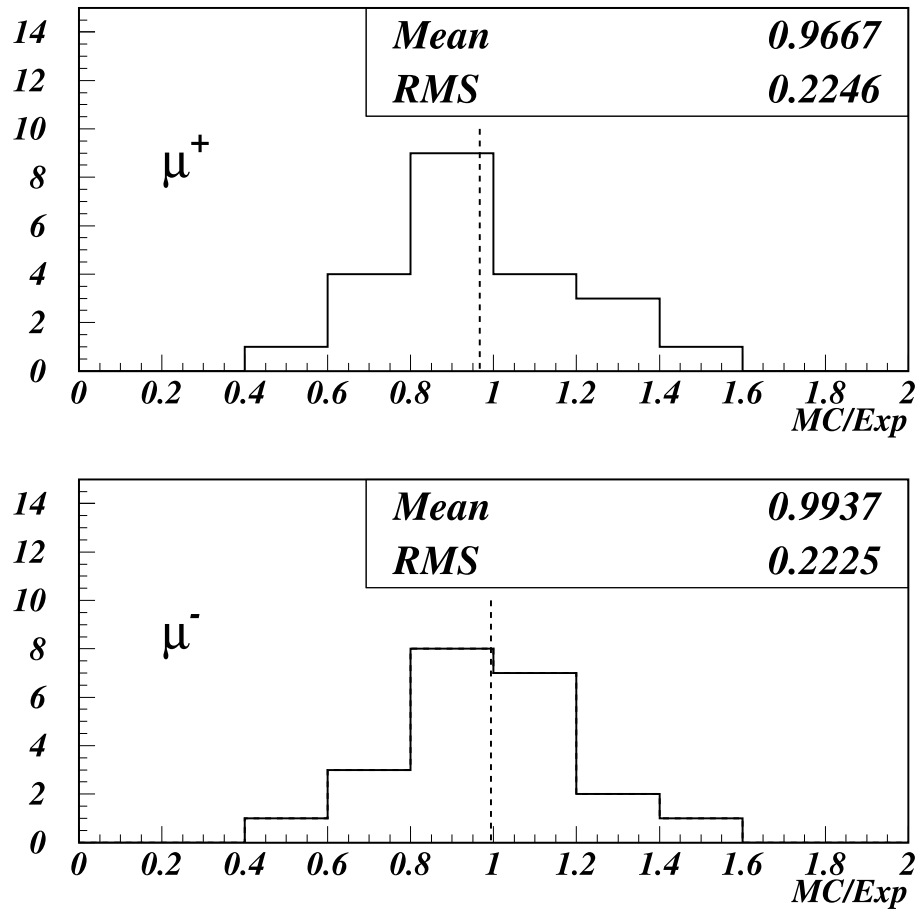

Figure 9: Distribution of the ratios of calculated to experimental muon flux at ground level for the different muon charges.

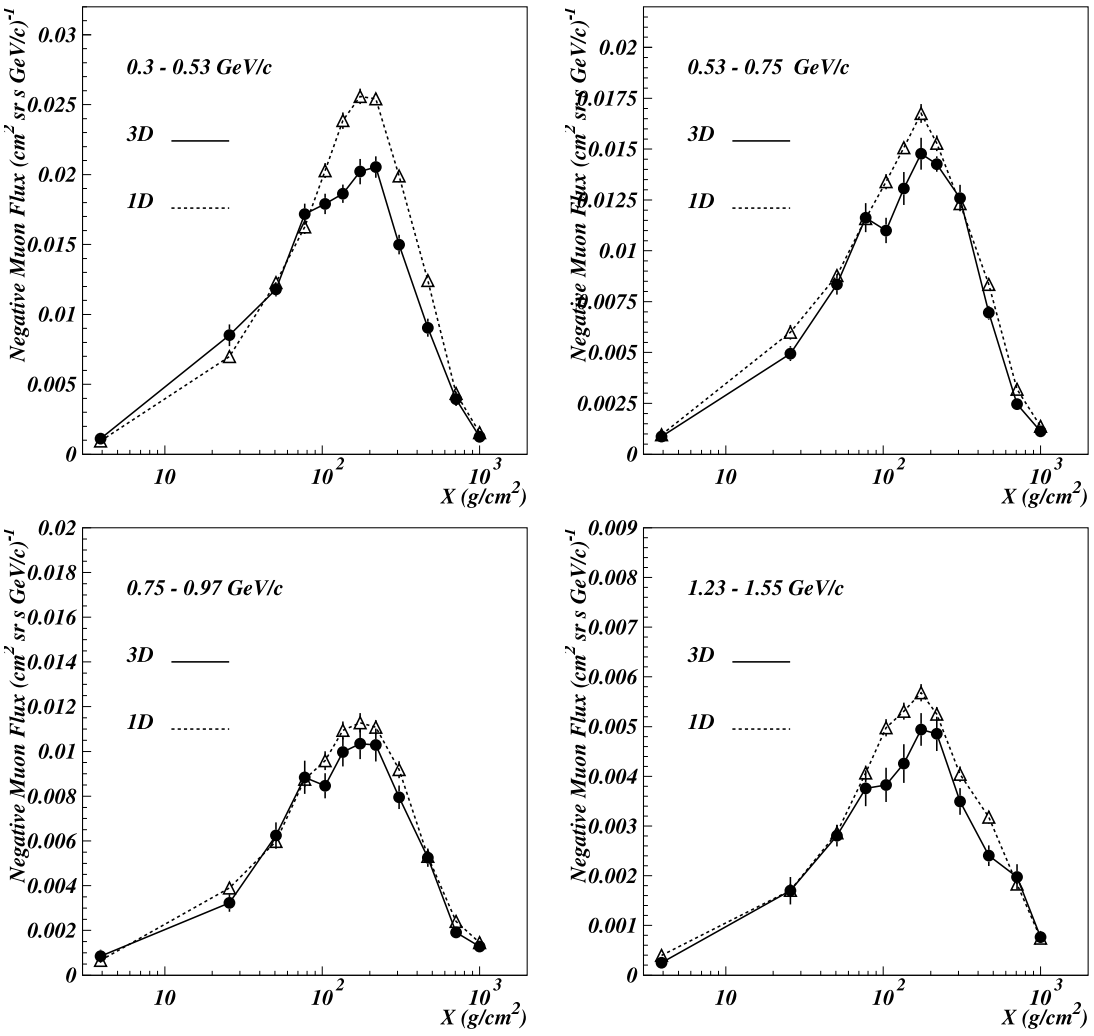

Figure 10: Comparison between 3–Dimensional and 1–Dimensional negative muon flux calculations as a function of atmospheric depth in a few different momentum ranges. The lines are drawn to guide the eye. case.

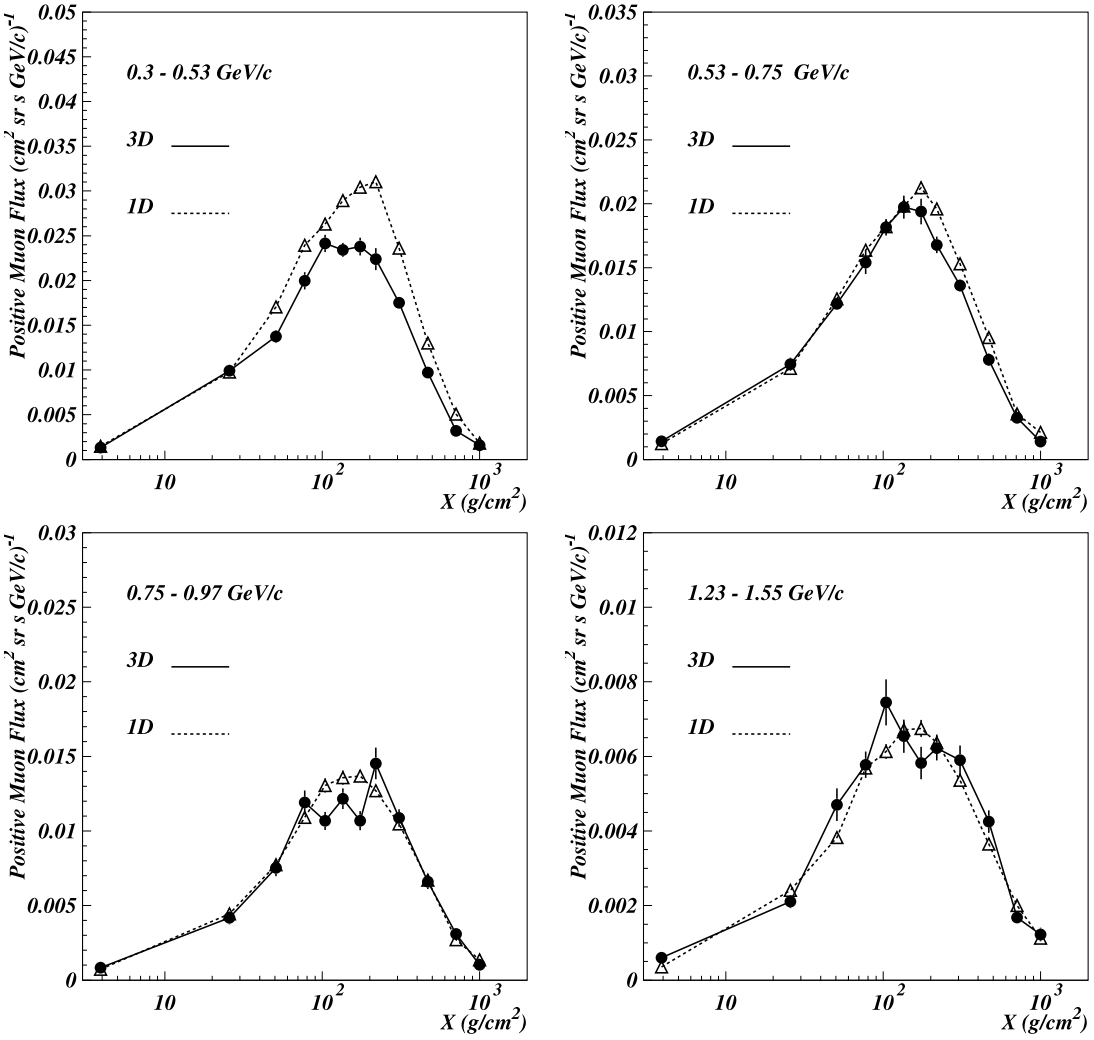

Figure 11: Comparison between 3–Dimensional and 1–Dimensional positive muon flux calculations as a function of atmospheric depth in a few different momentum ranges. The lines are drawn to guide the eye.

Appendix: Tables of numerical values

Table 3: Simulated negative muon flux as a function of momentum for the different depths in atmosphere.

Muon Mom. (GeV/c)	Flux (cm^2 s sr GeV/c)$^-1$	Flux (m^2 s sr GeV/c)$^-1$	Flux (m^2 s sr GeV/c)$^-1$
	3.9 g/cm^2	25.7 g/cm^2	50.7 g/cm^2
0.22	$9.31 \cdot 10^{-4} \pm 36$ %	$2.63 \cdot 10^{-3} \pm 19$ %	$7.93 \cdot 10^{-3} \pm 14$ %
0.28	$5.18 \cdot 10^{-4} \pm 31$ %	$6.04 \cdot 10^{-3} \pm 24$ %	$6.94 \cdot 10^{-3} \pm 15$ %
0.36	$1.92 \cdot 10^{-3} \pm 25$ %	$4.55 \cdot 10^{-3} \pm 24$ %	$9.45 \cdot 10^{-3} \pm 10$ %
0.45	$8.63 \cdot 10^{-4} \pm 25$ %	$2.85 \cdot 10^{-3} \pm 18$ %	$8.75 \cdot 10^{-3} \pm 12$ %
0.56	$1.17 \cdot 10^{-3} \pm 17$ %	$2.14 \cdot 10^{-3} \pm 17$ %	$4.68 \cdot 10^{-3} \pm 12$ %
0.71	$6.33 \cdot 10^{-4} \pm 22$ %	$1.85 \cdot 10^{-3} \pm 12$ %	$5.15 \cdot 10^{-3} \pm 13$ %
0.89	$8.43 \cdot 10^{-4} \pm 35$ %	$1.68 \cdot 10^{-3} \pm 12$ %	$3.23 \cdot 10^{-3} \pm 12$ %
1.12	$4.47 \cdot 10^{-4} \pm 32$ %	$9.58 \cdot 10^{-4} \pm 20$ %	$2.26 \cdot 10^{-3} \pm 13$ %
1.42	$2.52 \cdot 10^{-4} \pm 18$ %	$6.83 \cdot 10^{-4} \pm 18$ %	$1.70 \cdot 10^{-3} \pm 16$ %
1.78	$1.94 \cdot 10^{-4} \pm 24$ %	$3.84 \cdot 10^{-4} \pm 19$ %	$1.27 \cdot 10^{-3} \pm 9$ %
2.24	$1.10 \cdot 10^{-4} \pm 21$ %	$1.34 \cdot 10^{-4} \pm 23$ %	$6.74 \cdot 10^{-4} \pm 12$ %
2.83	$7.03 \cdot 10^{-5} \pm 37$ %	$8.21 \cdot 10^{-5} \pm 21$ %	$2.46 \cdot 10^{-4} \pm 16$ %
3.56	$2.72 \cdot 10^{-5} \pm 24$ %	$9.20 \cdot 10^{-5} \pm 22$ %	$1.84 \cdot 10^{-4} \pm 15$ %
4.48	$2.18 \cdot 10^{-5} \pm 30$ %	$5.22 \cdot 10^{-5} \pm 25$ %	$1.55 \cdot 10^{-4} \pm 15$ %
5.64	$6.62 \cdot 10^{-6} \pm 37$ %	$2.66 \cdot 10^{-5} \pm 18$ %	$6.18 \cdot 10^{-5} \pm 16$ %
7.10	$5.66 \cdot 10^{-6} \pm 26$ %	$1.29 \cdot 10^{-5} \pm 23$ %	$5.04 \cdot 10^{-5} \pm 23$ %
8.93	$1.13 \cdot 10^{-5} \pm 40$ %	$1.52 \cdot 10^{-5} \pm 30$ %	$3.44 \cdot 10^{-5} \pm 15$ %
11.25	$1.35 \cdot 10^{-6} \pm 40$ %	$3.83 \cdot 10^{-6} \pm 29$ %	$1.00 \cdot 10^{-5} \pm 22$ %
14.16	$3.46 \cdot 10^{-7} \pm 64$ %	$2.11 \cdot 10^{-6} \pm 30$ %	$5.93 \cdot 10^{-6} \pm 19$ %
17.83	$3.90 \cdot 10^{-7} \pm 37$ %	$1.34 \cdot 10^{-6} \pm 23$ %	$2.65 \cdot 10^{-6} \pm 17$ %
22.44	$1.37 \cdot 10^{-7} \pm 60$ %	$6.22 \cdot 10^{-7} \pm 26$ %	$3.11 \cdot 10^{-6} \pm 24$ %
28.25	$5.71 \cdot 10^{-8} \pm 63$ %	$4.84 \cdot 10^{-7} \pm 22$ %	$1.08 \cdot 10^{-6} \pm 30$ %
35.57	$7.24 \cdot 10^{-7} \pm 67$ %	$8.17 \cdot 10^{-7} \pm 59$ %	$1.26 \cdot 10^{-6} \pm 39$ %
44.77	$1.12 \cdot 10^{-8} \pm 54$ %	$1.56 \cdot 10^{-7} \pm 32$ %	$2.41 \cdot 10^{-7} \pm 24$ %
56.37	$3.62 \cdot 10^{-8} \pm 49$ %	$6.07 \cdot 10^{-8} \pm 46$ %	$9.43 \cdot 10^{-8} \pm 38$ %
70.96	$5.63 \cdot 10^{-9} \pm 52$ %	$2.97 \cdot 10^{-8} \pm 37$ %	$1.06 \cdot 10^{-7} \pm 31$ %
89.34	$5.20 \cdot 10^{-10} \pm 65$ %	$1.14 \cdot 10^{-9} \pm 35$ %	$8.23 \cdot 10^{-9} \pm 55$ %
112.47	$3.95 \cdot 10^{-10} \pm 68$ %	$2.47 \cdot 10^{-8} \pm 66$ %	$3.74 \cdot 10^{-8} \pm 47$ %
141.59	$5.13 \cdot 10^{-11} \pm 68$ %	$1.52 \cdot 10^{-8} \pm 61$ %	$1.56 \cdot 10^{-8} \pm 60$ %
178.25	$2.60 \cdot 10^{-10} \pm 61$ %	$1.15 \cdot 10^{-9} \pm 69$ %	$5.43 \cdot 10^{-9} \pm 41$ %
	77.3 g/cm^2	104.1 g/cm^2	135.3 g/cm^2
0.22	$9.24 \cdot 10^{-3} \pm 12$ %	$1.46 \cdot 10^{-2} \pm 7$ %	$1.79 \cdot 10^{-2} \pm 12$ %

continued on next page

continued from previous page

0.28	$1.44 \cdot 10^{-2} \pm 10$ %	$1.64 \cdot 10^{-2} \pm 10$ %	$1.72 \cdot 10^{-2} \pm 10$ %
0.36	$9.90 \cdot 10^{-3} \pm 10$ %	$1.78 \cdot 10^{-2} \pm 9$ %	$2.14 \cdot 10^{-2} \pm 6$ %
0.45	$1.16 \cdot 10^{-2} \pm 9$ %	$1.71 \cdot 10^{-2} \pm 10$ %	$1.56 \cdot 10^{-2} \pm 9$ %
0.56	$9.55 \cdot 10^{-3} \pm 8$ %	$1.29 \cdot 10^{-2} \pm 8$ %	$1.23 \cdot 10^{-2} \pm 6$ %
0.71	$7.40 \cdot 10^{-3} \pm 9$ %	$1.06 \cdot 10^{-2} \pm 8$ %	$9.94 \cdot 10^{-3} \pm 7$ %
0.89	$6.24 \cdot 10^{-3} \pm 9$ %	$8.84 \cdot 10^{-3} \pm 8$ %	$8.47 \cdot 10^{-3} \pm 7$ %
1.12	$3.67 \cdot 10^{-3} \pm 7$ %	$6.51 \cdot 10^{-3} \pm 7$ %	$6.80 \cdot 10^{-3} \pm 6$ %
1.42	$2.80 \cdot 10^{-3} \pm 8$ %	$3.76 \cdot 10^{-3} \pm 10$ %	$3.83 \cdot 10^{-3} \pm 9$ %
1.78	$1.81 \cdot 10^{-3} \pm 9$ %	$2.54 \cdot 10^{-3} \pm 10$ %	$2.70 \cdot 10^{-3} \pm 7$ %
2.24	$9.60 \cdot 10^{-4} \pm 11$ %	$1.23 \cdot 10^{-3} \pm 10$ %	$1.50 \cdot 10^{-3} \pm 8$ %
2.83	$5.56 \cdot 10^{-4} \pm 15$ %	$9.43 \cdot 10^{-4} \pm 12$ %	$1.18 \cdot 10^{-3} \pm 11$ %
3.56	$2.99 \cdot 10^{-4} \pm 14$ %	$4.69 \cdot 10^{-4} \pm 10$ %	$5.32 \cdot 10^{-4} \pm 8$ %
4.48	$3.35 \cdot 10^{-4} \pm 12$ %	$4.66 \cdot 10^{-4} \pm 10$ %	$5.35 \cdot 10^{-4} \pm 8$ %
5.64	$1.16 \cdot 10^{-4} \pm 14$ %	$1.64 \cdot 10^{-4} \pm 10$ %	$2.27 \cdot 10^{-4} \pm 8$ %
7.10	$6.80 \cdot 10^{-5} \pm 18$ %	$1.12 \cdot 10^{-4} \pm 14$ %	$1.39 \cdot 10^{-4} \pm 11$ %
8.93	$5.13 \cdot 10^{-5} \pm 16$ %	$6.49 \cdot 10^{-5} \pm 9$ %	$7.27 \cdot 10^{-5} \pm 8$ %
11.25	$2.55 \cdot 10^{-5} \pm 20$ %	$3.41 \cdot 10^{-5} \pm 17$ %	$3.66 \cdot 10^{-5} \pm 16$ %
14.16	$1.06 \cdot 10^{-5} \pm 15$ %	$1.53 \cdot 10^{-5} \pm 14$ %	$1.79 \cdot 10^{-5} \pm 13$ %
17.83	$4.52 \cdot 10^{-6} \pm 18$ %	$5.92 \cdot 10^{-6} \pm 16$ %	$7.16 \cdot 10^{-6} \pm 14$ %
22.44	$3.39 \cdot 10^{-6} \pm 18$ %	$3.86 \cdot 10^{-6} \pm 17$ %	$4.81 \cdot 10^{-6} \pm 17$ %
28.25	$2.29 \cdot 10^{-6} \pm 21$ %	$3.49 \cdot 10^{-6} \pm 20$ %	$3.86 \cdot 10^{-6} \pm 19$ %
35.57	$2.06 \cdot 10^{-6} \pm 25$ %	$2.42 \cdot 10^{-6} \pm 21$ %	$2.68 \cdot 10^{-6} \pm 21$ %
44.77	$3.88 \cdot 10^{-7} \pm 17$ %	$5.05 \cdot 10^{-7} \pm 17$ %	$5.54 \cdot 10^{-7} \pm 16$ %
56.37	$2.25 \cdot 10^{-7} \pm 31$ %	$3.93 \cdot 10^{-7} \pm 25$ %	$4.71 \cdot 10^{-7} \pm 22$ %
70.96	$1.96 \cdot 10^{-7} \pm 24$ %	$2.39 \cdot 10^{-7} \pm 21$ %	$2.43 \cdot 10^{-7} \pm 21$ %
89.34	$3.37 \cdot 10^{-8} \pm 29$ %	$4.87 \cdot 10^{-8} \pm 24$ %	$6.65 \cdot 10^{-8} \pm 22$ %
112.47	$3.98 \cdot 10^{-8} \pm 44$ %	$4.48 \cdot 10^{-8} \pm 39$ %	$6.10 \cdot 10^{-8} \pm 32$ %
141.59	$2.02 \cdot 10^{-8} \pm 51$ %	$3.00 \cdot 10^{-8} \pm 36$ %	$3.53 \cdot 10^{-8} \pm 32$ %
178.25	$6.61 \cdot 10^{-9} \pm 34$ %	$7.53 \cdot 10^{-9} \pm 32$ %	$9.32 \cdot 10^{-9} \pm 26$ %
	173.8 g/cm^2	218.8 g/cm^2	308.9 g/cm^2
0.22	$1.67 \cdot 10^{-2} \pm 12$ %	$1.53 \cdot 10^{-2} \pm 11$ %	$1.88 \cdot 10^{-2} \pm 12$ %
0.28	$1.80 \cdot 10^{-2} \pm 8$ %	$2.16 \cdot 10^{-2} \pm 8$ %	$2.12 \cdot 10^{-2} \pm 6$ %
0.36	$1.93 \cdot 10^{-2} \pm 8$ %	$2.16 \cdot 10^{-2} \pm 6$ %	$2.10 \cdot 10^{-2} \pm 9$ %
0.45	$1.85 \cdot 10^{-2} \pm 7$ %	$1.82 \cdot 10^{-2} \pm 8$ %	$1.91 \cdot 10^{-2} \pm 8$ %
0.56	$1.41 \cdot 10^{-2} \pm 9$ %	$1.64 \cdot 10^{-2} \pm 7$ %	$1.48 \cdot 10^{-2} \pm 6$ %
0.71	$1.22 \cdot 10^{-2} \pm 6$ %	$1.34 \cdot 10^{-2} \pm 7$ %	$1.38 \cdot 10^{-2} \pm 6$ %
0.89	$9.97 \cdot 10^{-3} \pm 6$ %	$1.03 \cdot 10^{-2} \pm 7$ %	$9.03 \cdot 10^{-3} \pm 7$ %
1.12	$7.34 \cdot 10^{-3} \pm 6$ %	$6.54 \cdot 10^{-3} \pm 7$ %	$6.77 \cdot 10^{-3} \pm 8$ %
1.42	$4.26 \cdot 10^{-3} \pm 9$ %	$4.94 \cdot 10^{-3} \pm 7$ %	$4.68 \cdot 10^{-3} \pm 5$ %

continued on next page

continued from previous page

1.78	$2.77 \cdot 10^{-3} \pm 8$ %	$2.59 \cdot 10^{-3} \pm 9$ %	$3.07 \cdot 10^{-3} \pm 8$ %
2.24	$1.66 \cdot 10^{-3} \pm 7$ %	$1.86 \cdot 10^{-3} \pm 8$ %	$1.86 \cdot 10^{-3} \pm 6$ %
2.83	$1.27 \cdot 10^{-3} \pm 10$ %	$1.27 \cdot 10^{-3} \pm 10$ %	$1.36 \cdot 10^{-3} \pm 7$ %
3.56	$6.36 \cdot 10^{-4} \pm 8$ %	$7.05 \cdot 10^{-4} \pm 9$ %	$8.80 \cdot 10^{-4} \pm 8$ %
4.48	$6.03 \cdot 10^{-4} \pm 7$ %	$5.28 \cdot 10^{-4} \pm 6$ %	$5.60 \cdot 10^{-4} \pm 6$ %
5.64	$2.58 \cdot 10^{-4} \pm 7$ %	$3.07 \cdot 10^{-4} \pm 8$ %	$3.21 \cdot 10^{-4} \pm 7$ %
7.10	$1.57 \cdot 10^{-4} \pm 11$ %	$1.67 \cdot 10^{-4} \pm 10$ %	$1.99 \cdot 10^{-4} \pm 10$ %
8.93	$8.34 \cdot 10^{-5} \pm 8$ %	$8.62 \cdot 10^{-5} \pm 8$ %	$9.93 \cdot 10^{-5} \pm 7$ %
11.25	$3.91 \cdot 10^{-5} \pm 15$ %	$4.72 \cdot 10^{-5} \pm 12$ %	$6.14 \cdot 10^{-5} \pm 10$ %
14.16	$1.99 \cdot 10^{-5} \pm 12$ %	$2.56 \cdot 10^{-5} \pm 10$ %	$2.56 \cdot 10^{-5} \pm 11$ %
17.83	$1.07 \cdot 10^{-5} \pm 14$ %	$1.00 \cdot 10^{-5} \pm 13$ %	$1.24 \cdot 10^{-5} \pm 13$ %
22.44	$5.32 \cdot 10^{-6} \pm 15$ %	$5.95 \cdot 10^{-6} \pm 14$ %	$7.37 \cdot 10^{-6} \pm 13$ %
28.25	$4.09 \cdot 10^{-6} \pm 18$ %	$5.50 \cdot 10^{-6} \pm 14$ %	$5.94 \cdot 10^{-6} \pm 13$ %
35.57	$3.45 \cdot 10^{-6} \pm 21$ %	$3.58 \cdot 10^{-6} \pm 20$ %	$3.98 \cdot 10^{-6} \pm 18$ %
44.77	$6.78 \cdot 10^{-7} \pm 15$ %	$7.14 \cdot 10^{-7} \pm 14$ %	$9.08 \cdot 10^{-7} \pm 14$ %
56.37	$6.09 \cdot 10^{-7} \pm 19$ %	$6.39 \cdot 10^{-7} \pm 19$ %	$7.44 \cdot 10^{-7} \pm 17$ %
70.96	$2.78 \cdot 10^{-7} \pm 20$ %	$3.10 \cdot 10^{-7} \pm 18$ %	$3.46 \cdot 10^{-7} \pm 19$ %
89.34	$9.49 \cdot 10^{-8} \pm 28$ %	$9.89 \cdot 10^{-8} \pm 27$ %	$1.08 \cdot 10^{-7} \pm 27$ %
112.47	$6.57 \cdot 10^{-8} \pm 29$ %	$7.03 \cdot 10^{-8} \pm 27$ %	$7.77 \cdot 10^{-8} \pm 27$ %
141.59	$3.61 \cdot 10^{-8} \pm 31$ %	$4.09 \cdot 10^{-8} \pm 28$ %	$4.62 \cdot 10^{-8} \pm 27$ %
178.25	$1.10 \cdot 10^{-8} \pm 23$ %	$1.31 \cdot 10^{-8} \pm 23$ %	$1.45 \cdot 10^{-8} \pm 22$ %
	463.7 g/cm^2	709.0 g/cm^2	1000.0 g/cm^2
0.22	$7.10 \cdot 10^{-3} \pm 15$ %	$9.52 \cdot 10^{-3} \pm 21$ %	$2.32 \cdot 10^{-3} \pm 13$ %
0.28	$1.09 \cdot 10^{-2} \pm 14$ %	$8.44 \cdot 10^{-3} \pm 9$ %	$4.00 \cdot 10^{-3} \pm 23$ %
0.36	$7.59 \cdot 10^{-3} \pm 10$ %	$9.48 \cdot 10^{-3} \pm 10$ %	$4.40 \cdot 10^{-3} \pm 16$ %
0.45	$9.05 \cdot 10^{-3} \pm 9$ %	$6.95 \cdot 10^{-3} \pm 10$ %	$3.54 \cdot 10^{-3} \pm 14$ %
0.56	$8.33 \cdot 10^{-3} \pm 6$ %	$7.92 \cdot 10^{-3} \pm 7$ %	$2.56 \cdot 10^{-3} \pm 13$ %
0.71	$5.87 \cdot 10^{-3} \pm 8$ %	$6.06 \cdot 10^{-3} \pm 9$ %	$2.39 \cdot 10^{-3} \pm 12$ %
0.89	$5.25 \cdot 10^{-3} \pm 8$ %	$4.59 \cdot 10^{-3} \pm 6$ %	$1.91 \cdot 10^{-3} \pm 11$ %
1.12	$3.56 \cdot 10^{-3} \pm 7$ %	$3.62 \cdot 10^{-3} \pm 7$ %	$1.34 \cdot 10^{-3} \pm 7$ %
1.42	$2.40 \cdot 10^{-3} \pm 9$ %	$2.16 \cdot 10^{-3} \pm 10$ %	$1.98 \cdot 10^{-3} \pm 13$ %
1.78	$2.16 \cdot 10^{-3} \pm 9$ %	$2.11 \cdot 10^{-3} \pm 8$ %	$1.26 \cdot 10^{-3} \pm 7$ %
2.24	$1.80 \cdot 10^{-3} \pm 8$ %	$1.69 \cdot 10^{-3} \pm 8$ %	$9.97 \cdot 10^{-4} \pm 9$ %
2.83	$9.90 \cdot 10^{-4} \pm 7$ %	$1.03 \cdot 10^{-3} \pm 8$ %	$6.98 \cdot 10^{-4} \pm 8$ %
3.56	$7.67 \cdot 10^{-4} \pm 8$ %	$6.86 \cdot 10^{-4} \pm 7$ %	$4.77 \cdot 10^{-4} \pm 10$ %
4.48	$3.62 \cdot 10^{-4} \pm 8$ %	$3.57 \cdot 10^{-4} \pm 8$ %	$3.24 \cdot 10^{-4} \pm 9$ %
5.64	$2.99 \cdot 10^{-4} \pm 5$ %	$3.00 \cdot 10^{-4} \pm 5$ %	$2.13 \cdot 10^{-4} \pm 10$ %
7.10	$1.39 \cdot 10^{-4} \pm 8$ %	$1.31 \cdot 10^{-4} \pm 9$ %	$1.10 \cdot 10^{-4} \pm 9$ %
8.93	$8.61 \cdot 10^{-5} \pm 8$ %	$8.50 \cdot 10^{-5} \pm 8$ %	$6.70 \cdot 10^{-5} \pm 9$ %

continued on next page

continued from previous page

11.25	$4.88 \cdot 10^{-5} \pm 9$ %	$4.81 \cdot 10^{-5} \pm 9$ %	$4.23 \cdot 10^{-5} \pm 12$ %
14.16	$2.72 \cdot 10^{-5} \pm 10$ %	$2.71 \cdot 10^{-5} \pm 10$ %	$2.57 \cdot 10^{-5} \pm 11$ %
17.83	$1.44 \cdot 10^{-5} \pm 12$ %	$1.41 \cdot 10^{-5} \pm 12$ %	$1.31 \cdot 10^{-5} \pm 13$ %
22.44	$1.08 \cdot 10^{-5} \pm 9$ %	$1.08 \cdot 10^{-5} \pm 9$ %	$1.05 \cdot 10^{-5} \pm 12$ %
28.25	$7.34 \cdot 10^{-6} \pm 13$ %	$7.37 \cdot 10^{-6} \pm 13$ %	$6.53 \cdot 10^{-6} \pm 12$ %
35.57	$3.50 \cdot 10^{-6} \pm 13$ %	$3.47 \cdot 10^{-6} \pm 13$ %	$3.41 \cdot 10^{-6} \pm 13$ %
44.77	$1.29 \cdot 10^{-6} \pm 13$ %	$1.40 \cdot 10^{-6} \pm 14$ %	$1.35 \cdot 10^{-6} \pm 14$ %
56.37	$9.40 \cdot 10^{-7} \pm 15$ %	$8.98 \cdot 10^{-7} \pm 16$ %	$9.15 \cdot 10^{-7} \pm 15$ %
70.96	$3.27 \cdot 10^{-7} \pm 18$ %	$3.27 \cdot 10^{-7} \pm 18$ %	$3.32 \cdot 10^{-7} \pm 18$ %
89.34	$1.67 \cdot 10^{-7} \pm 23$ %	$1.71 \cdot 10^{-7} \pm 23$ %	$1.66 \cdot 10^{-7} \pm 24$ %
112.47	$1.02 \cdot 10^{-7} \pm 21$ %	$1.03 \cdot 10^{-7} \pm 21$ %	$1.00 \cdot 10^{-7} \pm 22$ %
141.59	$5.60 \cdot 10^{-8} \pm 22$ %	$5.61 \cdot 10^{-8} \pm 22$ %	$5.15 \cdot 10^{-8} \pm 23$ %
178.25	$1.74 \cdot 10^{-8} \pm 19$ %	$1.76 \cdot 10^{-8} \pm 19$ %	$1.75 \cdot 10^{-8} \pm 19$ %

Table 4: Simulated positive muon flux as a function of momentum for the different depths in atmosphere.

Muon Mom. (GeV/c)	Flux (cm^2 s sr GeV/c)$^-1$	Flux (m^2 s sr GeV/c)$^-1$	Flux (m^2 s sr GeV/c)$^-1$
	3.9 g/cm^2	25.7 g/cm^2	50.7 g/cm^2
0.22	$8.18 \cdot 10^{-4} \pm 50$ %	$7.37 \cdot 10^{-3} \pm 18$ %	$1.47 \cdot 10^{-2} \pm 9$ %
0.28	$7.41 \cdot 10^{-4} \pm 27$ %	$1.08 \cdot 10^{-2} \pm 14$ %	$1.09 \cdot 10^{-2} \pm 13$ %
0.36	$9.79 \cdot 10^{-4} \pm 27$ %	$9.51 \cdot 10^{-3} \pm 11$ %	$1.34 \cdot 10^{-2} \pm 10$ %
0.45	$1.98 \cdot 10^{-3} \pm 32$ %	$9.67 \cdot 10^{-3} \pm 12$ %	$1.58 \cdot 10^{-2} \pm 7$ %
0.56	$6.18 \cdot 10^{-4} \pm 21$ %	$7.39 \cdot 10^{-3} \pm 7$ %	$1.31 \cdot 10^{-2} \pm 7$ %
0.71	$2.05 \cdot 10^{-3} \pm 19$ %	$7.52 \cdot 10^{-3} \pm 12$ %	$1.15 \cdot 10^{-2} \pm 7$ %
0.89	$8.24 \cdot 10^{-4} \pm 18$ %	$4.18 \cdot 10^{-3} \pm 10$ %	$7.53 \cdot 10^{-3} \pm 7$ %
1.12	$9.47 \cdot 10^{-4} \pm 21$ %	$2.81 \cdot 10^{-3} \pm 8$ %	$5.07 \cdot 10^{-3} \pm 8$ %
1.42	$6.02 \cdot 10^{-4} \pm 20$ %	$2.11 \cdot 10^{-3} \pm 8$ %	$4.70 \cdot 10^{-3} \pm 9$ %
1.78	$2.37 \cdot 10^{-4} \pm 28$ %	$1.81 \cdot 10^{-3} \pm 10$ %	$2.18 \cdot 10^{-3} \pm 10$ %
2.24	$2.20 \cdot 10^{-4} \pm 32$ %	$8.33 \cdot 10^{-4} \pm 16$ %	$1.51 \cdot 10^{-3} \pm 14$ %
2.83	$7.05 \cdot 10^{-5} \pm 23$ %	$5.32 \cdot 10^{-4} \pm 14$ %	$7.43 \cdot 10^{-4} \pm 10$ %
3.56	$8.84 \cdot 10^{-5} \pm 42$ %	$3.88 \cdot 10^{-4} \pm 12$ %	$5.60 \cdot 10^{-4} \pm 12$ %
4.48	$4.09 \cdot 10^{-5} \pm 35$ %	$1.50 \cdot 10^{-4} \pm 13$ %	$2.88 \cdot 10^{-4} \pm 12$ %
5.64	$8.99 \cdot 10^{-6} \pm 39$ %	$8.28 \cdot 10^{-5} \pm 11$ %	$1.43 \cdot 10^{-4} \pm 10$ %
7.10	$1.18 \cdot 10^{-5} \pm 50$ %	$4.28 \cdot 10^{-5} \pm 15$ %	$8.14 \cdot 10^{-5} \pm 13$ %
8.93	$3.02 \cdot 10^{-6} \pm 35$ %	$1.82 \cdot 10^{-5} \pm 21$ %	$4.00 \cdot 10^{-5} \pm 18$ %
11.25	$2.57 \cdot 10^{-6} \pm 33$ %	$1.35 \cdot 10^{-5} \pm 19$ %	$1.85 \cdot 10^{-5} \pm 17$ %
14.16	$1.34 \cdot 10^{-6} \pm 32$ %	$4.31 \cdot 10^{-6} \pm 22$ %	$7.12 \cdot 10^{-6} \pm 18$ %
17.83	$5.71 \cdot 10^{-8} \pm 37$ %	$6.60 \cdot 10^{-6} \pm 31$ %	$1.05 \cdot 10^{-5} \pm 20$ %
22.44	$5.31 \cdot 10^{-7} \pm 29$ %	$3.30 \cdot 10^{-6} \pm 18$ %	$4.23 \cdot 10^{-6} \pm 15$ %
28.25	$8.30 \cdot 10^{-8} \pm 53$ %	$1.32 \cdot 10^{-6} \pm 18$ %	$1.88 \cdot 10^{-6} \pm 17$ %
35.57	$8.85 \cdot 10^{-9} \pm 37$ %	$9.68 \cdot 10^{-7} \pm 25$ %	$1.44 \cdot 10^{-6} \pm 19$ %
44.77	$1.39 \cdot 10^{-8} \pm 46$ %	$3.09 \cdot 10^{-7} \pm 30$ %	$5.67 \cdot 10^{-7} \pm 22$ %
56.37	$2.90 \cdot 10^{-8} \pm 51$ %	$1.14 \cdot 10^{-7} \pm 36$ %	$3.83 \cdot 10^{-7} \pm 44$ %
70.96	$4.52 \cdot 10^{-8} \pm 57$ %	$7.48 \cdot 10^{-8} \pm 36$ %	$1.21 \cdot 10^{-7} \pm 26$ %
89.34	$1.09 \cdot 10^{-8} \pm 84$ %	$1.07 \cdot 10^{-7} \pm 64$ %	$1.33 \cdot 10^{-7} \pm 51$ %
112.47	$1.77 \cdot 10^{-9} \pm 77$ %	$3.24 \cdot 10^{-8} \pm 35$ %	$5.60 \cdot 10^{-8} \pm 28$ %
141.59	$0.00 \cdot 10^{0} \pm 0$ %	$3.21 \cdot 10^{-9} \pm 42$ %	$6.85 \cdot 10^{-9} \pm 28$ %
178.25	$0.00 \cdot 10^{0} \pm 0$ %	$1.99 \cdot 10^{-9} \pm 59$ %	$2.43 \cdot 10^{-9} \pm 48$ %
	77.3 g/cm^2	104.1 g/cm^2	135.3 g/cm^2
0.22	$1.76 \cdot 10^{-2} \pm 11$ %	$1.91 \cdot 10^{-2} \pm 9$ %	$1.99 \cdot 10^{-2} \pm 12$ %
0.28	$1.99 \cdot 10^{-2} \pm 9$ %	$2.23 \cdot 10^{-2} \pm 8$ %	$2.46 \cdot 10^{-2} \pm 8$ %
0.36	$2.20 \cdot 10^{-2} \pm 6$ %	$2.47 \cdot 10^{-2} \pm 8$ %	$2.51 \cdot 10^{-2} \pm 8$ %

continued on next page

continued from previous page

0.45	$1.84 \cdot 10^{-2} \pm 7$ %	$2.49 \cdot 10^{-2} \pm 5$ %	$2.13 \cdot 10^{-2} \pm 5$ %
0.56	$1.71 \cdot 10^{-2} \pm 9$ %	$1.76 \cdot 10^{-2} \pm 6$ %	$2.24 \cdot 10^{-2} \pm 7$ %
0.71	$1.41 \cdot 10^{-2} \pm 6$ %	$1.86 \cdot 10^{-2} \pm 6$ %	$1.76 \cdot 10^{-2} \pm 7$ %
0.89	$1.19 \cdot 10^{-2} \pm 7$ %	$1.07 \cdot 10^{-2} \pm 6$ %	$1.22 \cdot 10^{-2} \pm 6$ %
1.12	$8.09 \cdot 10^{-3} \pm 10$ %	$9.85 \cdot 10^{-3} \pm 6$ %	$1.06 \cdot 10^{-2} \pm 7$ %
1.42	$5.78 \cdot 10^{-3} \pm 6$ %	$7.45 \cdot 10^{-3} \pm 8$ %	$6.54 \cdot 10^{-3} \pm 7$ %
1.78	$3.34 \cdot 10^{-3} \pm 9$ %	$4.26 \cdot 10^{-3} \pm 9$ %	$4.70 \cdot 10^{-3} \pm 8$ %
2.24	$2.17 \cdot 10^{-3} \pm 9$ %	$2.62 \cdot 10^{-3} \pm 8$ %	$2.80 \cdot 10^{-3} \pm 10$ %
2.83	$1.11 \cdot 10^{-3} \pm 7$ %	$1.32 \cdot 10^{-3} \pm 8$ %	$1.24 \cdot 10^{-3} \pm 10$ %
3.56	$6.74 \cdot 10^{-4} \pm 8$ %	$9.12 \cdot 10^{-4} \pm 7$ %	$1.03 \cdot 10^{-3} \pm 7$ %
4.48	$3.92 \cdot 10^{-4} \pm 10$ %	$4.13 \cdot 10^{-4} \pm 10$ %	$4.70 \cdot 10^{-4} \pm 9$ %
5.64	$1.95 \cdot 10^{-4} \pm 9$ %	$2.15 \cdot 10^{-4} \pm 9$ %	$2.67 \cdot 10^{-4} \pm 8$ %
7.10	$1.30 \cdot 10^{-4} \pm 14$ %	$1.61 \cdot 10^{-4} \pm 12$ %	$1.88 \cdot 10^{-4} \pm 10$ %
8.93	$5.77 \cdot 10^{-5} \pm 14$ %	$6.88 \cdot 10^{-5} \pm 12$ %	$8.23 \cdot 10^{-5} \pm 11$ %
11.25	$2.46 \cdot 10^{-5} \pm 15$ %	$2.63 \cdot 10^{-5} \pm 12$ %	$3.10 \cdot 10^{-5} \pm 11$ %
14.16	$2.65 \cdot 10^{-5} \pm 21$ %	$3.35 \cdot 10^{-5} \pm 20$ %	$3.77 \cdot 10^{-5} \pm 16$ %
17.83	$1.33 \cdot 10^{-5} \pm 16$ %	$1.35 \cdot 10^{-5} \pm 15$ %	$1.67 \cdot 10^{-5} \pm 14$ %
22.44	$6.27 \cdot 10^{-6} \pm 19$ %	$9.10 \cdot 10^{-6} \pm 14$ %	$1.03 \cdot 10^{-5} \pm 13$ %
28.25	$3.59 \cdot 10^{-6} \pm 16$ %	$3.94 \cdot 10^{-6} \pm 15$ %	$4.36 \cdot 10^{-6} \pm 15$ %
35.57	$1.81 \cdot 10^{-6} \pm 19$ %	$3.24 \cdot 10^{-6} \pm 21$ %	$3.27 \cdot 10^{-6} \pm 21$ %
44.77	$8.21 \cdot 10^{-7} \pm 21$ %	$9.28 \cdot 10^{-7} \pm 20$ %	$9.98 \cdot 10^{-7} \pm 18$ %
56.37	$4.88 \cdot 10^{-7} \pm 35$ %	$9.58 \cdot 10^{-7} \pm 34$ %	$1.05 \cdot 10^{-6} \pm 30$ %
70.96	$1.43 \cdot 10^{-7} \pm 22$ %	$1.91 \cdot 10^{-7} \pm 21$ %	$2.19 \cdot 10^{-7} \pm 19$ %
89.34	$1.59 \cdot 10^{-7} \pm 43$ %	$1.74 \cdot 10^{-7} \pm 39$ %	$1.92 \cdot 10^{-7} \pm 35$ %
112.47	$6.66 \cdot 10^{-8} \pm 24$ %	$6.99 \cdot 10^{-8} \pm 22$ %	$7.90 \cdot 10^{-8} \pm 20$ %
141.59	$1.28 \cdot 10^{-8} \pm 21$ %	$1.38 \cdot 10^{-8} \pm 21$ %	$1.74 \cdot 10^{-8} \pm 17$ %
178.25	$3.13 \cdot 10^{-9} \pm 38$ %	$3.63 \cdot 10^{-9} \pm 33$ %	$3.93 \cdot 10^{-9} \pm 30$ %
	173.8 g/cm^2	218.8 g/cm^2	308.9 g/cm^2
0.22	$2.41 \cdot 10^{-2} \pm 11$ %	$2.01 \cdot 10^{-2} \pm 9$ %	$1.63 \cdot 10^{-2} \pm 7$ %
0.28	$2.32 \cdot 10^{-2} \pm 8$ %	$2.28 \cdot 10^{-2} \pm 7$ %	$1.56 \cdot 10^{-2} \pm 10$ %
0.36	$2.76 \cdot 10^{-2} \pm 5$ %	$2.03 \cdot 10^{-2} \pm 10$ %	$1.55 \cdot 10^{-2} \pm 7$ %
0.45	$2.12 \cdot 10^{-2} \pm 7$ %	$2.38 \cdot 10^{-2} \pm 6$ %	$2.03 \cdot 10^{-2} \pm 8$ %
0.56	$2.30 \cdot 10^{-2} \pm 8$ %	$1.95 \cdot 10^{-2} \pm 5$ %	$1.38 \cdot 10^{-2} \pm 4$ %
0.71	$1.65 \cdot 10^{-2} \pm 5$ %	$1.46 \cdot 10^{-2} \pm 6$ %	$1.35 \cdot 10^{-2} \pm 6$ %
0.89	$1.07 \cdot 10^{-2} \pm 6$ %	$1.45 \cdot 10^{-2} \pm 7$ %	$1.09 \cdot 10^{-2} \pm 5$ %
1.12	$1.14 \cdot 10^{-2} \pm 5$ %	$9.80 \cdot 10^{-3} \pm 5$ %	$7.66 \cdot 10^{-3} \pm 7$ %
1.42	$5.82 \cdot 10^{-3} \pm 8$ %	$6.22 \cdot 10^{-3} \pm 5$ %	$5.90 \cdot 10^{-3} \pm 7$ %
1.78	$4.80 \cdot 10^{-3} \pm 7$ %	$4.81 \cdot 10^{-3} \pm 6$ %	$4.44 \cdot 10^{-3} \pm 9$ %
2.24	$2.68 \cdot 10^{-3} \pm 7$ %	$2.36 \cdot 10^{-3} \pm 5$ %	$2.08 \cdot 10^{-3} \pm 9$ %

continued on next page

continued from previous page

2.83	$1.47 \cdot 10^{-3} \pm 9$ %	$1.72 \cdot 10^{-3} \pm 7$ %	$1.43 \cdot 10^{-3} \pm 7$ %
3.56	$1.10 \cdot 10^{-3} \pm 6$ %	$9.81 \cdot 10^{-4} \pm 8$ %	$9.55 \cdot 10^{-4} \pm 7$ %
4.48	$5.58 \cdot 10^{-4} \pm 10$ %	$5.23 \cdot 10^{-4} \pm 9$ %	$5.03 \cdot 10^{-4} \pm 7$ %
5.64	$3.08 \cdot 10^{-4} \pm 7$ %	$3.30 \cdot 10^{-4} \pm 7$ %	$3.23 \cdot 10^{-4} \pm 9$ %
7.10	$1.91 \cdot 10^{-4} \pm 9$ %	$2.09 \cdot 10^{-4} \pm 7$ %	$2.31 \cdot 10^{-4} \pm 8$ %
8.93	$8.20 \cdot 10^{-5} \pm 12$ %	$9.27 \cdot 10^{-5} \pm 10$ %	$1.07 \cdot 10^{-4} \pm 8$ %
11.25	$4.10 \cdot 10^{-5} \pm 10$ %	$4.26 \cdot 10^{-5} \pm 10$ %	$5.97 \cdot 10^{-5} \pm 7$ %
14.16	$4.17 \cdot 10^{-5} \pm 14$ %	$4.78 \cdot 10^{-5} \pm 13$ %	$4.84 \cdot 10^{-5} \pm 10$ %
17.83	$2.35 \cdot 10^{-5} \pm 11$ %	$2.61 \cdot 10^{-5} \pm 11$ %	$2.97 \cdot 10^{-5} \pm 11$ %
22.44	$1.11 \cdot 10^{-5} \pm 12$ %	$1.22 \cdot 10^{-5} \pm 11$ %	$1.21 \cdot 10^{-5} \pm 10$ %
28.25	$4.86 \cdot 10^{-6} \pm 14$ %	$5.48 \cdot 10^{-6} \pm 14$ %	$5.99 \cdot 10^{-6} \pm 12$ %
35.57	$4.24 \cdot 10^{-6} \pm 18$ %	$5.17 \cdot 10^{-6} \pm 16$ %	$5.36 \cdot 10^{-6} \pm 16$ %
44.77	$1.16 \cdot 10^{-6} \pm 17$ %	$1.20 \cdot 10^{-6} \pm 16$ %	$1.28 \cdot 10^{-6} \pm 15$ %
56.37	$1.07 \cdot 10^{-6} \pm 30$ %	$1.21 \cdot 10^{-6} \pm 26$ %	$1.29 \cdot 10^{-6} \pm 25$ %
70.96	$2.49 \cdot 10^{-7} \pm 18$ %	$3.87 \cdot 10^{-7} \pm 24$ %	$3.99 \cdot 10^{-7} \pm 22$ %
89.34	$2.03 \cdot 10^{-7} \pm 33$ %	$1.38 \cdot 10^{-7} \pm 16$ %	$1.77 \cdot 10^{-7} \pm 17$ %
112.47	$8.56 \cdot 10^{-8} \pm 19$ %	$1.01 \cdot 10^{-7} \pm 16$ %	$1.03 \cdot 10^{-7} \pm 13$ %
141.59	$2.02 \cdot 10^{-8} \pm 15$ %	$2.48 \cdot 10^{-8} \pm 16$ %	$3.41 \cdot 10^{-8} \pm 16$ %
178.25	$4.51 \cdot 10^{-9} \pm 26$ %	$5.38 \cdot 10^{-9} \pm 23$ %	$6.58 \cdot 10^{-9} \pm 21$ %
	463.7 g/cm^2	709.0 g/cm^2	1000.0 g/cm^2
0.22	$7.57 \cdot 10^{-3} \pm 12$ %	$3.69 \cdot 10^{-3} \pm 26$ %	$7.71 \cdot 10^{-4} \pm 23$ %
0.28	$9.69 \cdot 10^{-3} \pm 13$ %	$2.27 \cdot 10^{-3} \pm 16$ %	$1.47 \cdot 10^{-3} \pm 28$ %
0.36	$9.22 \cdot 10^{-3} \pm 11$ %	$3.61 \cdot 10^{-3} \pm 11$ %	$1.56 \cdot 10^{-3} \pm 18$ %
0.45	$1.01 \cdot 10^{-2} \pm 9$ %	$3.45 \cdot 10^{-3} \pm 17$ %	$1.68 \cdot 10^{-3} \pm 21$ %
0.56	$7.99 \cdot 10^{-3} \pm 8$ %	$3.66 \cdot 10^{-3} \pm 11$ %	$1.48 \cdot 10^{-3} \pm 16$ %
0.71	$7.65 \cdot 10^{-3} \pm 11$ %	$2.94 \cdot 10^{-3} \pm 8$ %	$1.33 \cdot 10^{-3} \pm 16$ %
0.89	$6.60 \cdot 10^{-3} \pm 7$ %	$3.09 \cdot 10^{-3} \pm 12$ %	$1.02 \cdot 10^{-3} \pm 11$ %
1.12	$4.67 \cdot 10^{-3} \pm 6$ %	$2.31 \cdot 10^{-3} \pm 8$ %	$1.12 \cdot 10^{-3} \pm 14$ %
1.42	$4.25 \cdot 10^{-3} \pm 7$ %	$1.68 \cdot 10^{-3} \pm 9$ %	$1.23 \cdot 10^{-3} \pm 15$ %
1.78	$2.24 \cdot 10^{-3} \pm 5$ %	$1.28 \cdot 10^{-3} \pm 11$ %	$7.07 \cdot 10^{-4} \pm 12$ %
2.24	$1.91 \cdot 10^{-3} \pm 9$ %	$1.20 \cdot 10^{-3} \pm 9$ %	$5.80 \cdot 10^{-4} \pm 12$ %
2.83	$1.28 \cdot 10^{-3} \pm 6$ %	$6.84 \cdot 10^{-4} \pm 9$ %	$5.15 \cdot 10^{-4} \pm 13$ %
3.56	$6.77 \cdot 10^{-4} \pm 7$ %	$5.11 \cdot 10^{-4} \pm 9$ %	$3.68 \cdot 10^{-4} \pm 10$ %
4.48	$4.79 \cdot 10^{-4} \pm 9$ %	$3.48 \cdot 10^{-4} \pm 10$ %	$3.04 \cdot 10^{-4} \pm 9$ %
5.64	$3.22 \cdot 10^{-4} \pm 8$ %	$2.57 \cdot 10^{-4} \pm 8$ %	$2.05 \cdot 10^{-4} \pm 8$ %
7.10	$1.95 \cdot 10^{-4} \pm 7$ %	$1.42 \cdot 10^{-4} \pm 9$ %	$8.94 \cdot 10^{-5} \pm 11$ %
8.93	$8.71 \cdot 10^{-5} \pm 9$ %	$7.82 \cdot 10^{-5} \pm 10$ %	$6.78 \cdot 10^{-5} \pm 9$ %
11.25	$6.17 \cdot 10^{-5} \pm 7$ %	$5.93 \cdot 10^{-5} \pm 10$ %	$5.92 \cdot 10^{-5} \pm 14$ %
14.16	$5.42 \cdot 10^{-5} \pm 12$ %	$4.91 \cdot 10^{-5} \pm 12$ %	$3.62 \cdot 10^{-5} \pm 10$ %

continued on next page

continued from previous page

17.83	$2.48 \cdot 10^{-5} \pm 11$ %	$2.13 \cdot 10^{-5} \pm 14$ %	$2.02 \cdot 10^{-5} \pm 17$ %
22.44	$1.21 \cdot 10^{-5} \pm 10$ %	$1.13 \cdot 10^{-5} \pm 11$ %	$9.70 \cdot 10^{-6} \pm 13$ %
28.25	$6.08 \cdot 10^{-6} \pm 11$ %	$7.42 \cdot 10^{-6} \pm 13$ %	$7.21 \cdot 10^{-6} \pm 14$ %
35.57	$5.60 \cdot 10^{-6} \pm 20$ %	$4.27 \cdot 10^{-6} \pm 17$ %	$3.96 \cdot 10^{-6} \pm 15$ %
44.77	$1.14 \cdot 10^{-6} \pm 16$ %	$1.15 \cdot 10^{-6} \pm 16$ %	$9.98 \cdot 10^{-7} \pm 15$ %
56.37	$1.35 \cdot 10^{-6} \pm 24$ %	$1.33 \cdot 10^{-6} \pm 24$ %	$1.30 \cdot 10^{-6} \pm 25$ %
70.96	$4.08 \cdot 10^{-7} \pm 22$ %	$4.05 \cdot 10^{-7} \pm 22$ %	$4.06 \cdot 10^{-7} \pm 22$ %
89.34	$2.19 \cdot 10^{-7} \pm 15$ %	$2.70 \cdot 10^{-7} \pm 15$ %	$2.61 \cdot 10^{-7} \pm 16$ %
112.47	$8.56 \cdot 10^{-8} \pm 14$ %	$8.55 \cdot 10^{-8} \pm 15$ %	$9.34 \cdot 10^{-8} \pm 15$ %
141.59	$3.48 \cdot 10^{-8} \pm 16$ %	$3.59 \cdot 10^{-8} \pm 15$ %	$2.88 \cdot 10^{-8} \pm 14$ %
178.25	$1.55 \cdot 10^{-8} \pm 22$ %	$1.56 \cdot 10^{-8} \pm 23$ %	$1.57 \cdot 10^{-8} \pm 22$ %

Table 5: Simulated muon flux as a function of momentum at ground depth.

Muon Mom. (GeV/c)	μ^+ Flux (cm^2 s sr GeV/c)$^-$1	μ^- Flux (cm^2 s sr GeV/c)$^-$1
0.22	$7.71 \cdot 10^{-4} \pm 23$ %	$7.79 \cdot 10^{-4} \pm 24$ %
0.28	$1.47 \cdot 10^{-3} \pm 28$ %	$8.05 \cdot 10^{-4} \pm 17$ %
0.36	$1.56 \cdot 10^{-3} \pm 18$ %	$1.09 \cdot 10^{-3} \pm 20$ %
0.45	$1.68 \cdot 10^{-3} \pm 21$ %	$1.64 \cdot 10^{-3} \pm 16$ %
0.56	$1.48 \cdot 10^{-3} \pm 16$ %	$8.01 \cdot 10^{-4} \pm 15$ %
0.71	$1.33 \cdot 10^{-3} \pm 16$ %	$1.38 \cdot 10^{-3} \pm 10$ %
0.89	$1.02 \cdot 10^{-3} \pm 11$ %	$1.29 \cdot 10^{-3} \pm 16$ %
1.12	$1.12 \cdot 10^{-3} \pm 14$ %	$1.26 \cdot 10^{-3} \pm 14$ %
1.42	$1.23 \cdot 10^{-3} \pm 15$ %	$7.66 \cdot 10^{-4} \pm 12$ %
1.78	$7.07 \cdot 10^{-4} \pm 12$ %	$7.35 \cdot 10^{-4} \pm 12$ %
2.24	$5.80 \cdot 10^{-4} \pm 12$ %	$6.77 \cdot 10^{-4} \pm 11$ %
2.83	$5.15 \cdot 10^{-4} \pm 13$ %	$4.32 \cdot 10^{-4} \pm 12$ %
3.56	$3.68 \cdot 10^{-4} \pm 10$ %	$3.21 \cdot 10^{-4} \pm 9$ %
4.48	$3.04 \cdot 10^{-4} \pm 9$ %	$2.88 \cdot 10^{-4} \pm 10$ %
5.64	$2.05 \cdot 10^{-4} \pm 8$ %	$1.31 \cdot 10^{-4} \pm 11$ %
7.10	$8.94 \cdot 10^{-5} \pm 11$ %	$9.28 \cdot 10^{-5} \pm 8$ %
8.93	$6.78 \cdot 10^{-5} \pm 9$ %	$5.49 \cdot 10^{-5} \pm 9$ %
11.25	$5.92 \cdot 10^{-5} \pm 14$ %	$3.68 \cdot 10^{-5} \pm 11$ %
14.16	$3.62 \cdot 10^{-5} \pm 10$ %	$1.98 \cdot 10^{-5} \pm 13$ %
17.83	$2.02 \cdot 10^{-5} \pm 17$ %	$1.32 \cdot 10^{-5} \pm 12$ %
22.44	$9.70 \cdot 10^{-6} \pm 13$ %	$9.17 \cdot 10^{-6} \pm 13$ %
28.25	$7.21 \cdot 10^{-6} \pm 14$ %	$5.39 \cdot 10^{-6} \pm 15$ %
35.57	$3.96 \cdot 10^{-6} \pm 15$ %	$3.39 \cdot 10^{-6} \pm 14$ %
44.77	$9.98 \cdot 10^{-7} \pm 15$ %	$1.27 \cdot 10^{-6} \pm 14$ %
56.37	$1.30 \cdot 10^{-6} \pm 25$ %	$8.44 \cdot 10^{-7} \pm 15$ %
70.96	$4.06 \cdot 10^{-7} \pm 22$ %	$3.27 \cdot 10^{-7} \pm 18$ %
89.34	$2.61 \cdot 10^{-7} \pm 16$ %	$1.69 \cdot 10^{-7} \pm 24$ %
112.47	$9.34 \cdot 10^{-8} \pm 15$ %	$9.80 \cdot 10^{-8} \pm 21$ %
141.59	$2.88 \cdot 10^{-8} \pm 14$ %	$5.12 \cdot 10^{-8} \pm 23$ %
178.25	$1.57 \cdot 10^{-8} \pm 22$ %	$1.49 \cdot 10^{-8} \pm 19$ %